PHYSICS

Pattern recognition with neuromorphic computing using magnetic field–induced dynamics of skyrmions

Tomoyuki Yokouchi[1,2]*, Satoshi Sugimoto[3], Bivas Rana[1,4], Shinichiro Seki[1,5,6,7], Naoki Ogawa[1,5,6], Yuki Shiomi[2], Shinya Kasai[3,5], Yoshichika Otani[1,8,9]

Nonlinear phenomena in physical systems can be used for brain-inspired computing with low energy consumption. Response from the dynamics of a topological spin structure called skyrmion is one of the candidates for such a neuromorphic computing. However, its ability has not been well explored experimentally. Here, we experimentally demonstrate neuromorphic computing using nonlinear response originating from magnetic field–induced dynamics of skyrmions. We designed a simple-structured skyrmion-based neuromorphic device and succeeded in handwritten digit recognition with the accuracy as large as 94.7% and waveform recognition. Notably, there exists a positive correlation between the recognition accuracy and the number of skyrmions in the devices. The large degrees of freedom of skyrmion systems, such as the position and the size, originate from the more complex nonlinear mapping, the larger output dimension, and, thus, high accuracy. Our results provide a guideline for developing energy-saving and high-performance skyrmion neuromorphic computing devices.

INTRODUCTION

Artificial neural networks, mimicking human brains, exhibit extraordinary abilities in several tasks, such as image recognition (*1*), machine translation (*2*), and a board game (*3*). Nowadays, most artificial neural networks rely on silicon-based general-purpose electronic circuits, such as a central processing unit and a graphics processing unit. However, these circuits consume a large amount of energy and are approaching the physical limits of downscaling (*4*). Therefore, developing devices specialized for brain-inspired computing, namely, neuromorphic devices, is highly required (*4*, *5*). In particular, nonlinearity and short-term memory effects are essential functions for neuromorphic devices that various spintronic devices can offer (*6*–*21*). Among them, we focus on a topological spin structure called magnetic skyrmion (*22*–*31*). So far, skyrmion-based neuromorphic devices, such as reservoir computing devices (*9*–*14*), synapse devices (*15*, *16*), and probabilistic computing devices (*17*, *18*), have been studied to bring about high performance. However, a fully experimental evaluation of its ability for neuromorphic tasks such as pattern recognition is still lacking.

We design the skyrmion neuromorphic computer on the basis of a reservoir computing model (*7*–*13*, *32*–*39*). The conventional reservoir computing model consists of two parts (Fig. 1A). The first part, called the "reservoir part," performs a complex nonlinear transformation of input data into high-dimensional output data. Here, the dimension is the number of linearly independent outputs. In this process, the reservoir part temporally stores the information of past input to make the output depend on both present and past inputs (short-term memory effect). The second part conducts a linear transformation of the outputs from the reservoir part. The coefficient parameters of this linear transformation are optimized by using a training dataset so that the final output becomes a desirable one. Incidentally, the nonlinear transformation of input into high-dimensional outputs is the essence of reservoir computing; the linearly inseparable data can become linearly separable in the high-dimensional space, enabling complex data classification as in the kernel method (*40*). Optimizing parameters (i.e., training) in reservoir computing is unnecessary for the reservoir part. In other words, the reservoir part performs the complex nonlinear transformation with fixed parameters. Hence, we can implement the reservoir part using a physical system with the complex nonlinearity and memory effect (or equally hysteresis) with short-term properties (*7*–*13*, *33*–*37*). As shown below, skyrmion systems also exhibit nonlinearity and short-term memory effects. Moreover, the skyrmion system has large degrees of freedom because each can take various states with different positions and sizes. This feature theoretically brings about a complex transformation of input data and high performance (*9*–*13*). However, it has not been experimentally explored well. We experimentally found that the skyrmion-based physical reservoir device exhibits good abilities in recognition tasks. Notably, although the structure of the present device is quite simple, the recognition accuracy as high as 94.7% is obtained in a handwritten digit recognition task, indicating an advantage of the skyrmion system in neuromorphic computing.

RESULTS

Our skyrmion-based physical device consists of parallelly connected "subsections" (Fig. 1, B to D). A subsection is a simple-shaped Hall bar made of Pt/Co/Ir film deposited on SiO_2/Si substrate, in which skyrmions appear (*41*–*43*). Each subsection has single input and output. The input signal is a time-dependent out-of-plane magnetic field [$H_{AC}(t)$] whose waveform is the same as what we want to compute. The output is an anomalous Hall voltage [$V(t)$], which changes in response to $H_{AC}(t)$ because of the $H_{AC}(t)$-induced change in magnetic structures. We note that the magnitude of the topological Hall effect is much smaller than that of the anomalous Hall effect

[1]RIKEN Center for Emergent Matter Science (CEMS), Wako 351-0198, Japan. [2]Department of Basic Science, The University of Tokyo, Tokyo 152-8902, Japan. [3]National Institute for Materials Science (NIMS), Tsukuba 305-0047, Japan. [4]Institute of Spintronics and Quantum Information, Faculty of Physics, Adam Mickiewicz University, Poznań, Uniwersytetu Poznanskiego 2, Poznań 61-614, Poland. [5]PRESTO, Japan Science and Technology Agency (JST), Tokyo 102-0075, Japan. [6]Department of Applied Physics, The University of Tokyo, Tokyo 113-8656, Japan. [7]Institute of Engineering Innovation, The University of Tokyo, Tokyo 113-8656, Japan. [8]Institute for Solid State Physics (ISSP), The University of Tokyo, Kashiwa 277-8561, Japan. [9]Trans-scale Quantum Science Institute, University of Tokyo, Bunkyo-ku, Tokyo 113-0033, Japan.
*Corresponding author. Email: yokouchi@g.ecc.u-tokyo.ac.jp

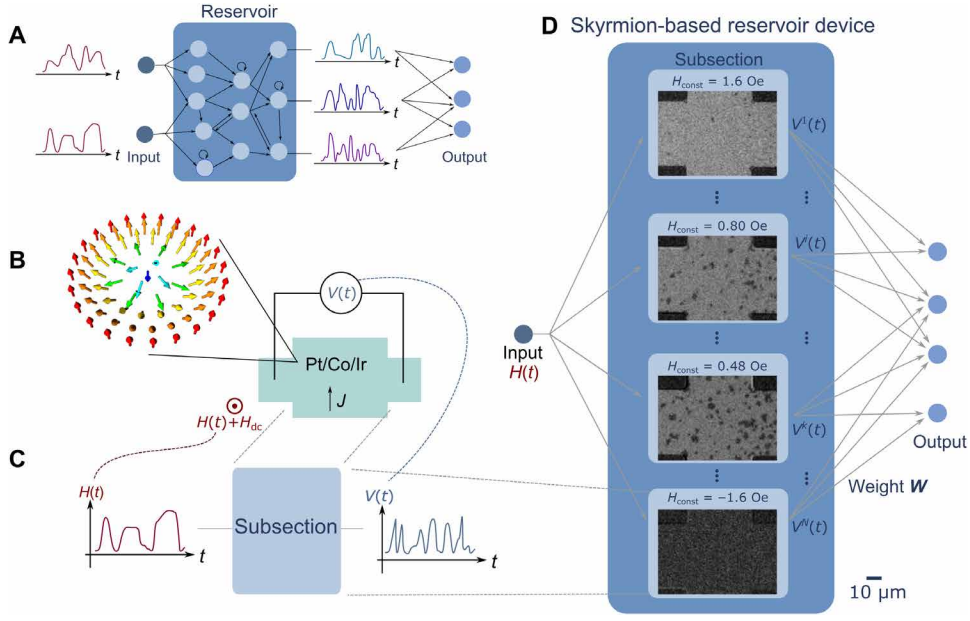

Fig. 1. Concept of skyrmion-based neuromorphic computing. (**A**) Schematic for the conventional reservoir computing model. (**B**) Schematic illustration of a Hall bar device and a magnetic skyrmion. (**C**) Conceptual diagram for the data conversion in a subsection. (**D**) Schematic illustration of a skyrmion-based neuromorphic computer. Polar Kerr images of the subsection with various constant magnetic fields (H_{const}) in the absence of a time-dependent magnetic field [$H_{AC}(t)$] are also presented.

since the size of the skyrmion is large—a few micrometers. As shown later, in this process, $V(t)$ depends on the past input signal and is nonlinear to $H_{AC}(t)$ as required in a physical reservoir. Then, we parallelly connect N subsections, in which the different magnitude of a constant out-of-plane magnetic field (H_{const}) is applied (Fig. 1D). Because the magnetic structures differ depending on H_{const} (fig. S1), the output signals from the subsections tend to be linearly independent of each other. We input the same signal into N subsections. Hence, the skyrmion-based neuromorphic computer device nonlinearly converts a one-dimensional time-series input [$H_{AC}(t)$] to a linearly independent N-dimensional time-series outputs [$\boldsymbol{V}(t) \in \mathbb{R}^N$] as follows

$$H_{AC}(t) \rightarrow \boldsymbol{V}(t)$$

$$\boldsymbol{V}(t) = [V^1(t), \cdots, V^N(t)]$$

Here, $V^i(t)$ is the output signal of the ith subsection. This nonlinear mapping into the high-dimensional space is crucial for skyrmion-based neuromorphic computing like conventional reservoir computing. The final output is a linear combination of sampling data from $\boldsymbol{V}(t)$. The linear combination coefficients are optimized using a training dataset to ensure that the final output is desirable (see Materials and Methods for details). We used only one Hall bar in the actual measurement and obtained $V(t)$ by repeating the measurement N times for the same $H_{AC}(t)$ with H_{const} changed. All experiments were performed at room temperature.

First, we present basic properties of response in a single subsection, which shows short-term memory effect and nonlinearity. Figure 2 (A to D) shows the time dependence of the input magnetic field $H_{AC}(t)$ and the output anomalous Hall voltage $V(t)$. When we applied two cycles of a sine wave magnetic field, $V(t)$ exhibited distinct variation (Fig. 2C). This change originates from the magnetic field–induced transformation of the spin structure. As shown in Fig. 2 (E to H), the size, form, and the number of skyrmions vary in response to $H_{AC}(t)$, and consequently, the total magnetization in the Hall bar area also varies, which leads to the observed change in $V(t)$. We note that the magnitude of $H_{AC}(t)$ required for saturating the magnetization is larger than that of H_{const} because the magnetic structure cannot totally follow $H_{AC}(t)$. Besides, the $V(t)$ signal depends on a past input; when we change the first cycle of the input signal from the sine wave to a square wave, as shown in Fig. 2B, the time profile of $V(t)$ differs from that in the case of two cycles of the sine wave (see Fig. 2, C and D). In particular, the second cycle of the input signal is a sine wave in both cases; however, $V(t)$ profiles corresponding to the second cycle are substantially different. In other words, the output signal depends on the past input signal (i.e., memory effect). This memory effect is due to the history-dependent time evolution of the spin structures originating from the first-order transition nature of the skyrmion system. As shown in Fig. 2 (E to L), the time evolution of spin structure for the first cycle differs between the sine and square waves (Fig. 2, F and J). As a result, the spin structure during the second cycle of $H_{AC}(t)$ is also different in two cases (Fig. 2, G and K), which makes $V(t)$ dependent on past inputs.

Moreover, the memory effect in the skyrmion system has a short-term property. In other words, after turning off the input signal, the output signal fades out and goes back to an initial value. As shown in fig. S2, after two cycles of the sine wave are input, the output signals start to return to an intimal value, which indicates that the skyrmion system has the short-term memory property. We note that the time to return the initial state depends strongly on H_{const}, and in some H_{const} values, the time is more than several tens of seconds. We also investigate the nonlinearity in $V(t)$ versus $H_{AC}(t)$. We measured the output anomalous Hall voltage $V(t)$ when two cycles of sine wave magnetic field with various amplitudes were

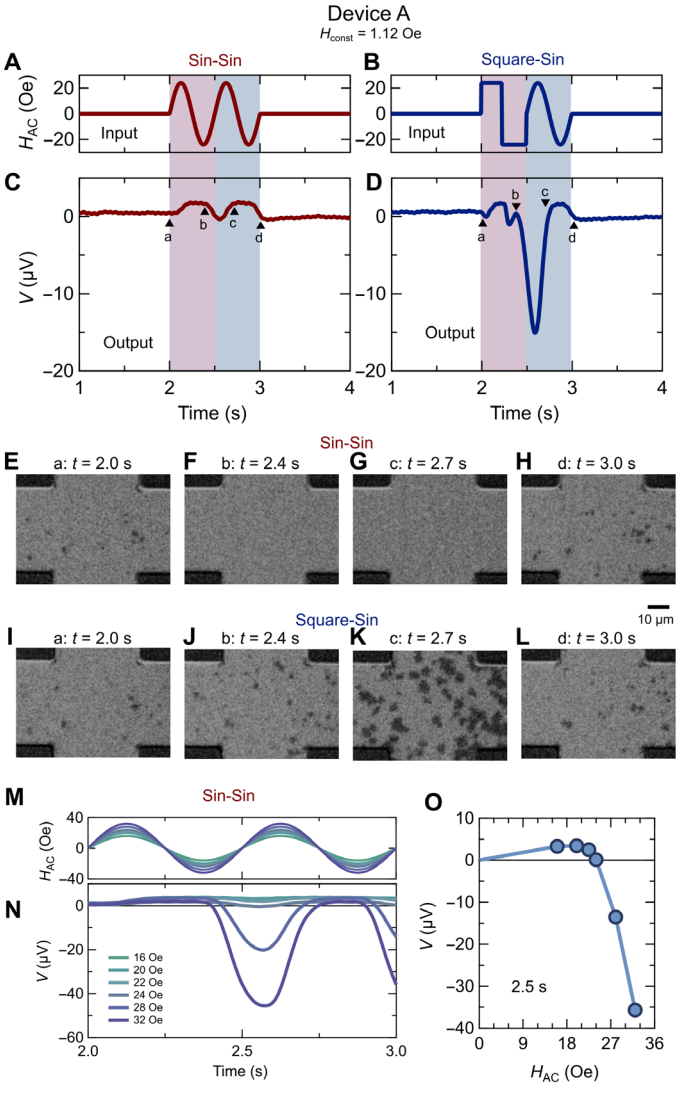

Fig. 2. Memory effect and nonlinearity in the skyrmion system. (**A** to **D**) The time profile of the input magnetic field (H_{AC}) (A and B) and the corresponding Hall voltage (C and D) in the Hall bar device A with the constant magnetic field H_{const} = 1.12 Oe. (**E** to **L**) Snapshots of polar Kerr images during the application of H_{AC} for the Sin-Sin input (E to H) and the Square-Sin input (I to L).. The corresponding time points are represented in (C) and (D) by the triangles. (**M** and **N**) The time profile of H_{AC} with various amplitudes (M) and the corresponding Hall voltage output (N) in the Hall bar device A with the constant magnetic field H_{const} = 1.12 Oe. (**O**) The Hall voltage output at t = 2.5 s as a function of the amplitude of H_{AC}. The solid line is a guide for eyes.

applied (Fig. 2, M and N). The magnitude of $V(t)$ at t = 2.5 s as a function of the amplitude of the input magnetic field is presented in Fig. 2O. The $V(t)$ is not proportional to the amplitude and even shows the sign change, which indicates the strong nonlinearity of the output anomalous Hall voltage to the input magnetic field as required in a physical reservoir.

Next, we demonstrate a waveform classification task, widely used as a benchmark task for neuromorphic computing (*7*, *38*, *39*). In this task, the input signal is a waveform of a random combination of sine and square waves (Fig. 3A), and the desired output is 1 for the sine waves and −1 for the square waves. We input the waveform in Fig. 3A into the skyrmion-based reservoir device with N = 41 subsections. The amplitude of $H_{AC}(t)$ is 24 Oe. Before inputting the signal, we create the ferromagnetic state by applying a large magnetic field to erase the memory of previous inputs. As an example, $V^i(t)$ signals outputted from some subsections (H_{const} = 1.04, 0.00 and −1.60 Oe) are displayed in Fig. 3B; the input data are complicatedly transformed, and their profiles differ in different subsections as expected. We sampled the output signals with the sampling rate of 100 Hz and calculated the final output as $y(t_k) = \sum_{i=1}^{41} W_i V^i(t_k)$, where W_i (i = 1,2, ⋯ ,41) is the time-independent coefficient, and t_k is the time at the kth sampling point (see also Materials and Methods). Then, W_i is optimized by using the first half of the waveform (0 to 25 s) so that the mean squared error between $y(t_k)$ and the target value is the minimum, and finally, we binarized $y(t_k)$ (see Materials and Methods for details). As shown in Fig. 3 (C and D), the output values follow the desired output values well not only in the input dataset used for the training (0 to 25 s) but also in the dataset not used for the training (25 to 50 s).

To investigate the effect of the skyrmion formation on the recognition accuracy, we fabricate the Hall bar devices accommodating fewer skyrmions and ferromagnetic-like domains (devices B to D) as shown in Fig. 3E by controlling the strength of perpendicular magnetic anisotropy (PMA) (see Materials and Methods). Here, the magnitude of PMA gradually decreases from device D to device A. Then, we performed the same waveform recognition task with various amplitudes of $H_{AC}(t)$. As shown in Fig. 3F, the recognition accuracy in device A, which has the largest skyrmion population of the four devices, is high. In contrast, device D, which accommodates ferromagnetic domains, exhibits low recognition accuracy for all $H_{AC}(t)$ amplitudes. We count the number of skyrmions existing during the waveform recognition task $\langle n_{sk} \rangle$ (see Materials and Methods for details); as shown in Fig. 3G, we found a large $\langle n_{sk} \rangle$ in device A and a small number in device D as expected. Figure 3H shows the correlation between the recognition accuracy and $\langle n_{sk} \rangle$, exhibiting a positive correlation. This result suggests that the skyrmion formation is critical in improving recognition accuracy.

Before discussing the origin of better recognition accuracy in the skyrmion system, we demonstrate that the skyrmion-based reservoir device can solve a more complex task: handwritten digit recognition. We use the commonly used Mixed National Institute of Standards and Technology database (MNIST) (*44*), some examples of which are shown in Fig. 4F. A preprocessing was performed to convert a two-dimensional image to a one-dimensional input signal (see Materials and Methods for details). Figure 4 (A to D) shows the preprocessing for an input digit "5," as an example. We input the converted signal into the skyrmion-based reservoir device (device A) with N = 9 subsections. The output signals corresponding to the input digit "5" are presented in Fig. 4E. The final output is obtained by a post-facto linear transformation of the output signals from each subsection, in which 9 × 176 × 10 weights were used (see Materials and Methods for details). Using 13,219 train images, we optimize the coefficients of the linear transformation. After the optimization, 5000 test images not included in the train dataset are used to test the recognition accuracy. Figure 4G presents a confusion matrix obtained in the test process, which shows that the skyrmion-based reservoir outputs desired digits well. The recognition accuracy is 94.7 ± 0.3%. This accuracy is better than an experiment in tungsten oxide (WOx) memristors–based reservoir device (88.1%) (*33*), simulation in a nanowire-based reservoir system (90%) (*37*),

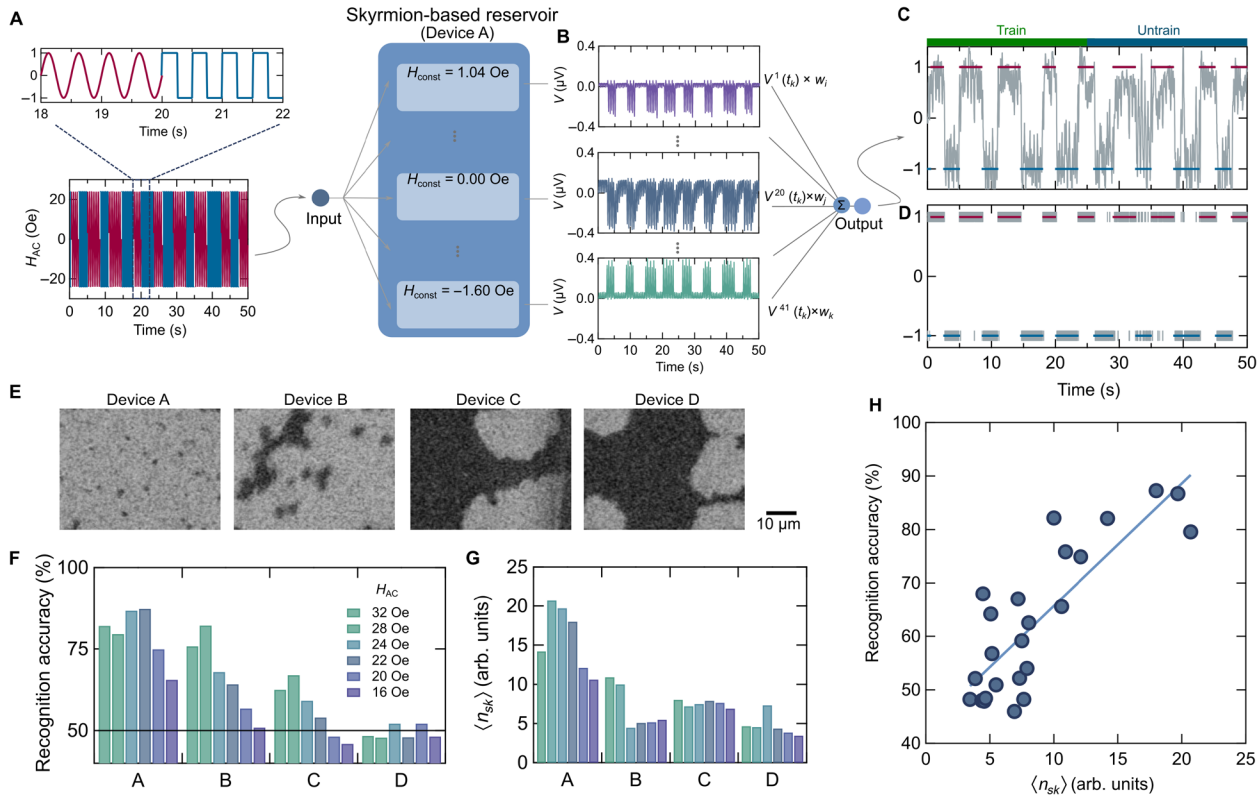

Fig. 3. Waveform recognition task. (**A**) The waveform of input signal [$H_{AC}(t)$] for the waveform recognition task. The input signal is a waveform of a random combination of sine (red) and square waves (blue). (**B**) The output signals (V) in some of the subsections with different constant magnetic fields (H_{const}). (**C** and **D**) The final output calculated by the linear combination of the output signals in the 41 subsections (C) and its binarization (D). The blue and red lines are the desired output. (**E**) Polar Kerr images of devices A to D. The thicknesses of the Co layer in devices A, B, C, and D are 0.655, 0.656, 0.657, and 0.658 nm, respectively. (**F**) The recognition accuracy in the waveform recognition task for devices A to D for various amplitudes of H_{AC}. (**G**) The average number of skyrmions $\langle n_{sk} \rangle$ during the waveform recognition task for devices A to D for various amplitudes of H_{AC}. (**H**) A scatterplot of $\langle n_{sk} \rangle$ and the recognition rate. A correlation coefficient of 0.82 is obtained.

and chip-level simulation in a skyrmion-based artificial synapse system (89%) (*15*). We note that when we directly performed the linear transformation of the preprocessing data without skyrmion-based reservoir devices, the recognition accuracy is 9.9 ± 0.4%.

DISCUSSION

Last, we discuss the origin of the better recognition accuracy obtained using the skyrmion-based neuromorphic device than the ferromagnetic domain–based one. First, the creep motion of ferromagnetic domains decreases the recognition accuracy. In fig. S3, we present the 41 output signals (H_{const} = −1.6 to 1.6 Oe) in the waveform recognition task for skyrmions (device A) and ferromagnetic domains (device C). In the case of ferromagnetic domains, the center of the oscillation (the red lines in fig. S3F) gradually changes with time at low H_{const}. This tendency originates from a slow change in the total magnetization in the Hall bar due to the thermally induced creep motion of the ferromagnetic domains. Such a gradual change in the background must reduce the recognition accuracy because even if we input the same signal, the outputs might be different depending on time, causing false recognition. In contrast, in the case of skyrmion (device A), the output signals oscillate around the time-independent values. This is because thermal agitation has a lower impact on the magnetization in the skyrmion-based device (i.e., the total number of skyrmions) compared with the magnetization in the ferromagnetic domain–based device due to the topological stability of skyrmions (i.e., a finite energy barrier between skyrmions and ferromagnetic state). Hence, the profiles of the output signals are reproducible and determined by the form of the input signal. As shown in fig. S4 and Supplementary Text, the output signals and the number of skyrmions are reproducible. Although some skyrmions are created/annihilated stochastically because of the thermal effect, the stochastic fluctuations are averaged out since many skyrmions exist in the device.

Second, the larger number of output data dimensions, which originates from the large degree of freedoms of the skyrmion system, also contributes to better recognition accuracy. As mentioned above, the complex nonlinear mapping into high-dimensional space is a crucial factor for the present neuromorphic computing. Because of the particle nature of skyrmions, skyrmion systems have many degrees of freedom, such as position and skyrmion size, causing different spin structural responses to the input signals $H_{AC}(t)$. This results in high-dimensional mapping. However, the ferromagnetic domain state consists of only two internal states (up and down domains). Hence, the transformation should be less complex than the skyrmion system. To further discuss the dimensionality, we evaluate the dimensionality of the experimentally obtained output signals. The dimensionality is defined by the linearly independent

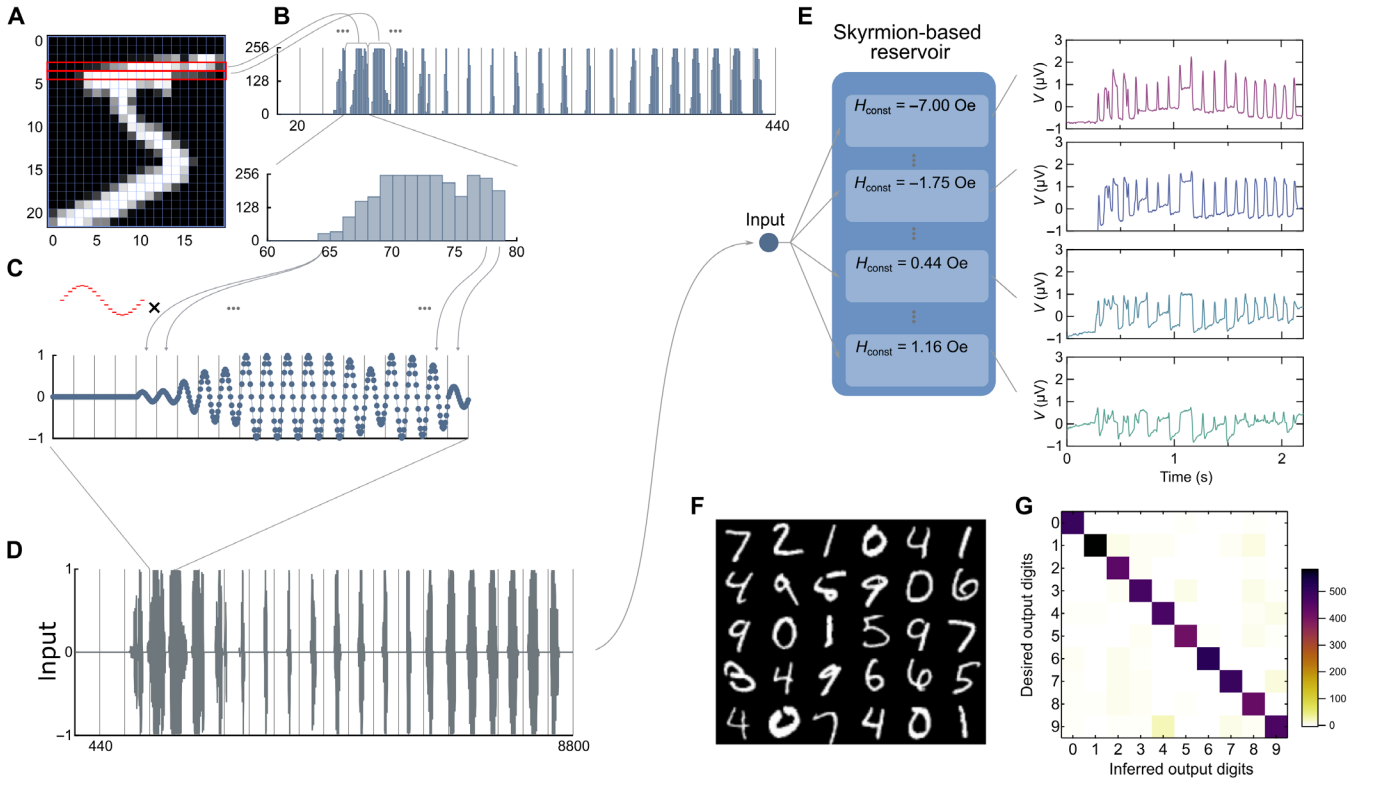

Fig. 4. Handwritten digits recognition task. (**A** to **D**) Schematic for preprocessing for the handwritten digits recognition task. The two-dimensional image (A) is converted to a one-dimensional array (B). A sine wave is multiplied by each data point (C), and an input signal is obtained (D) (see also Materials and Methods for details). (**E**) The output signals from subsections corresponding to the input digit "5." (**F**) Some examples from the MNIST database. (**G**) A confusion matrix showing the recognition results from the skyrmion-based reservoir versus the desired outputs. A recognition accuracy of 94.7 ± 0.3% is obtained.

outputs from the subsections. Thus, we plot an output signal of the *i*th subsection (V^i) obtained in the waveform recognition task as a function of an output signal of the *j*th subsection with a different H_{const} value (V^j) ($i \neq j$) (fig. S5). If V^i and V^j are linearly dependent (i.e., $V^i = CV^j$, where C is a coefficient), the profile becomes a straight line. However, if V^i and V^j are linearly independent, the curve shape becomes nonmonotonous. As shown in fig. S5A, the profiles for the skyrmion-based device tend to be nonmonotonous smooth curves. In contrast, the ferromagnetic domain–based device profiles are relatively straight and squarish (fig. S5C). These results indicate that the number of linearly independent outputs in the skyrmion-based device is more than that in the ferromagnetic domain device. In other words, the skyrmion-based device has a larger dimensionality than the ferromagnetic domain–based device. This fact contributes to the better recognition accuracy in the skyrmion-based device.

We experimentally conclude that the skyrmion system is a promising candidate for neuromorphic computing. The high degree of freedom and topological stability of the skyrmions lead to reproducible, complex, and high-dimensional mapping and, consequently, better recognition accuracy. The present skyrmion-based neuromorphic system consists of less than 10 simple-shaped and microscale Hall bars. Nevertheless, the recognition accuracy in the handwritten digit recognition task is better than other neuromorphic devices (*15*, *33*, *37*), which require the fabrication of a large number of nanoscale objects. Moreover, using nanometric skyrmions (*45*), current-induced dynamics of skyrmions (*12*, *46*), and magnetic tunnel junctions (*47*) can further improve the performance. In addition, other spin textures with high degrees of freedom and the stability against thermal agitation, such as anti-skyrmions (*48*) and skyrmion strings (*49*), might also be used for the neuromorphic system. Our findings provide a previously unknown pathway for designing a high-performance neuromorphic computer.

MATERIALS AND METHODS

Device fabrications

We deposited multilayer films on SiO_2/Si substrates by DC and radio frequency (RF) magnetron sputtering. The complete stack structure of the films used in this work is SiO_2/Si substrates/Ta (5 nm)/Pt (5 nm)/Co (d_{Co})/Ir (0.8 nm)/Pt (5 nm) in which the nominal thickness of Co (d_{Co}) gradually varies from 0.6 to 0.7 nm. The Co layer was deposited by using DC sputtering, and the other materials were deposited by RF sputtering. Thermodynamically stable skyrmions form in an area with $d_{Co} \sim 0.65$ nm, and ferromagnetic domains are observed in a thicker area. This is because d_{Co} affects the PMA, which determines the stable spin structure as investigated in our previous works (*41*–*43*). Next, we patterned the films by using maskless ultraviolet lithography followed by Ar ion milling. The width of the Hall bars is 40 μm.

Waveform recognition

Waveform recognition task is divided into two parts: (i) the transformation of an input signal by using the physical neuromorphic

device and (ii) a linear transformation of the signals output from the neuromorphic device and optimization of their weights. For the first part, we input a time-dependent magnetic field $H_{const} + H_{AC}(t)$. Here, H_{const} is a constant out-of-plane magnetic field in order to make a magnetic structure in each subsection a different one, which results in the linearly independent outputs as mentioned in the results section. The wave profile of $H_{AC}(t)$ corresponds to the signal that we want to process and is a random combination of sine and square waves as shown in Fig. 3A in this case. We generate $H_{const} + H_{AC}(t)$ by applying the current to a coil with the use of a function generator (NF WF1974) and a bipolar amplifier (NF HSA42011). The direction of the magnetic field is perpendicular to the film plane. The consequent time-dependent Hall voltage $[V(t)]$ is measured with lock-in techniques (NF LI5650) by applying AC with current density $j = 2.5 \times 10^8$ Am^{-2} and frequency $f = 333$ Hz. The skyrmion-based neuromorphic computer used here has 41 subsections with different H_{const} values. Thus, we obtain the converted signals as follows: $\boldsymbol{V}(t_k) = [V^1(t_k), \cdots, V^{41}(t_k)]$. Here, $V^i(t)$ is the output signal of the ith subsection, and t_k is time at the kth sampling point. We sampled the data with the frequency of 100 Hz (i.e., $k = 1,2, \cdots, 5000$ and $t_0 = 0$, $t_1 = 0.01, \cdots, t_k = 0.01k, \cdots, t_{5000} = 50$ s).

The second part is performed on a conventional computer. The final output signal is the linear combination of $\boldsymbol{V}(t_k)$ as follows: $y(t_k) = \sum_{i=1}^{41} W_i V^i(t_k)$. Here, W_i is the time-independent coefficient and is optimized to minimize the mean square error $\sum_{k=1}^{2500} [y(t_k) - L(t_k)]^2$. The label $L(t_k)$ is 1 when the input signal is the sine wave and −1 when the input signal is the square wave (Fig. 3, C and D). For the optimization, we use the first half of the dataset (i.e., 2500 data obtained from $t = 0$ to 25 s). Last, we binarized the $y(t_k)$.

Count of the skyrmion number during the waveform recognition task

The number of skyrmions depends on the device number (A to D) and the amplitude of the input signals $[H_{AC}(t)]$. During the waveform recognition task, we take a video of time evolution of magnetic contrast with the use of a poler Kerr microscopy. The exposure time is approximately 50 ms. Then, we count the number of skyrmions by using a conventional binarization method. Here, we defined a particle whose size is below 6 by 6 μm^2 as a skyrmion. Last, the number of skyrmions is normalized by the area of the Hall bar and the execution time of the task, and $\langle n_{sk} \rangle$ is obtained.

Handwritten digit recognition

The handwritten digit recognition task is divided into three parts: (i) transformation of two-dimensional data into one-dimensional input data, (ii) nonlinear transformation of an input signal by using the skyrmion-based reservoir computing device, and (iii) a linear transformation of the output signals from the reservoir and optimization of their weights.

At the beginning of the first part, we removed the unused border area of the images by reducing the original 28 × 28 images into a 22 × 20 image (Fig. 4A). Then, we reshaped the two-dimensional 22 × 20 data points to one-dimensional 440 data points (Fig. 4B). In the next step, we multiply each data point by one cycle of sine wave consisting of 20 data points and obtained a sequence of 440 modulated sine waves (Fig. 4, C and D) (i.e., the number of total data points is 8800).

In the second part, we input a time-dependent magnetic field $H_{const} + H_{AC}(t)$ into the skyrmion-based neuromorphic device with nine different H_{const} values. The amplitude of $H_{AC}(t)$ is 64 Oe for four subsections and 70 Oe for five subsections. The frequency is 200 Hz. The consequent time-dependent Hall voltage $[V(t)]$ is measured with lock-in techniques by applying AC current with current density $j = 2.5 \times 10^8$ Am^{-2} and frequency $f = 2.99$ kHz. The sampling rate is 80 Hz. Then, the output signal for the dth data is obtained as follows: $\boldsymbol{V}_d = (V_d^1(t_k), \cdots, V_d^i(t_k), \cdots, V_d^9(t_k))$, where t_k is time at the kth sampling point, i.e., $k = 1,2, \cdots, 176$ and $t_0 = 0$, $t_1 = 0.0125, \cdots, t_k = 0.0125k, \cdots, t_{176} = 2.2$ s , and 9 is the number of subsections.

Last, we calculate the final output for the dth dataset as follows

$$\boldsymbol{y}^d = \boldsymbol{V}_d \mathrm{W} = \left(V_d^1(t_0), \cdots V_d^1(t_{176}), \cdots, V_d^9(t_0), \cdots, V_d^9(t_{176})\right)$$

$$\begin{pmatrix} W_{1,1} & \cdots & W_{1,10} \\ \vdots & \ddots & \vdots \\ W_{1584,1} & \cdots & W_{1584,10} \end{pmatrix}$$

Here, the output $\boldsymbol{y}^d$ is a 1 × 10 vector, and W is a 1584 × 10 weight matrix. Then, we introduce the 1 × 10 label vector $\boldsymbol{L}^d$. If the dth input data are a digit of m, the mth components of $\boldsymbol{L}^d$ are one, and the others, zero. We optimize to minimize the mean square error $\sum_{d=1}^{13219} \| \boldsymbol{y}^d - \boldsymbol{L}^d \|^2$ by using 13,219 train data. In the test process, we calculate $\boldsymbol{y}^d$, and the predicted digit is determined from the maximum component of $\boldsymbol{y}^d$. For evaluation of the recognition accuracy, 5000 test images that are not included in the train dataset are used. To reduce the ambiguity due to a choice of test and train data, we repeated optimization 10 times with different choices of test and train data and take the average. The choice of train and test images is fully random. As shown in fig. S6A, the recognition accuracy increases with the increasing number of train images and is already saturated at 13,219 train data. In addition, the recognition accuracy also increases with the increasing number of subsections N (fig. S6B). We note that the total experimental time for one subsection is 2.2 s × 18,219 = 11.1 hours.

SUPPLEMENTARY MATERIALS

Supplementary material for this article is available at https://science.org/doi/10.1126/sciadv.abq5652

REFERENCES AND NOTES

1. A. Krizhevsky, I. Sutskever, G. E. Hinton, ImageNet classification with deep convolutional neural networks, in *Advances in Neural Information Processing Systems*, F. Pereira, C. J. Burges, L. Bottou, K. Q. Weinberger, Eds. (Curran Associates Inc., 2012), vol. 25, p. 1097.
2. Y. LeCun, Y. Bengio, G. Hinton, Deep learning. *Nature* **521**, 436–444 (2015).
3. D. Silver, A. Huang, C. J. Maddison, A. Guez, L. Sifre, G. van den Driessche, J. Schrittwieser, I. Antonoglou, V. Panneershelvam, M. Lanctot, S. Dieleman, D. Grewe, J. Nham, N. Kalchbrenner, I. Sutskever, T. Lillicrap, M. Leach, K. Kavukcuoglu, T. Graepel, D. Hassabis, Mastering the game of Go with deep neural networks and tree search. *Nature* **529**, 484–489 (2016).
4. K. Roy, A. Jaiswal, P. Panda, Towards spike-based machine intelligence with neuromorphic computing. *Nature* **575**, 607–617 (2019).
5. C. Kaspar, B. J. Ravoo, W. G. van der Wiel, S. V. Wegner, W. H. P. Pernice, The rise of intelligent matter. *Nature* **594**, 345–355 (2021).
6. J. Grollier, D. Querlioz, K. Y. Camsari, K. Everschor-Sitte, S. Fukami, M. D. Stiles, Neuromorphic spintronics. *Nat. Electron.* **3**, 360–370 (2020).
7. G. Tanaka, T. Yamane, J. B. Héroux, R. Nakane, N. Kanazawa, S. Takeda, H. Numata, D. Nakano, A. Hirose, Recent advances in physical reservoir computing: A review. *Neural Netw.* **115**, 100–123 (2019).
8. J. Torrejon, M. Riou, F. A. Araujo, S. Tsunegi, G. Khalsa, D. Querlioz, P. Bortolotti, V. Cros, K. Yakushiji, A. Fukushima, H. Kubota, S. Yuasa, M. D. Stiles, J. Grollier, Neuromorphic computing with nanoscale spintronic oscillators. *Nature* **547**, 428–431 (2017).

9. D. Prychynenko, M. Sitte, K. Litzius, B. Krüger, G. Bourianoff, M. Kläui, J. Sinova, K. Everschor-Sitte, Magnetic skyrmion as a nonlinear resistive element: A potential building block for reservoir computing. *Phys. Rev. Appl.* **9**, 014034 (2018).
10. G. Bourianoff, D. Pinna, M. Sitte, K. Everschor-Sitte, Potential implementation of reservoir computing models based on magnetic skyrmions. *AIP Adv.* **8**, 055602 (2018).
11. W. Jiang, L. Chen, K. Zhou, L. Li, Q. Fu, Y. Du, R. H. Liu, Physical reservoir computing using magnetic skyrmion memristor and spin torque nano-oscillator. *Appl. Phys. Lett.* **115**, 192403 (2019).
12. D. Pinna, G. Bourianoff, K. Everschor-Sitte, Reservoir computing with random skyrmion textures. *Phys. Rev. Applied* **14**, 054020 (2020).
13. X. Chen, F. A. Araujo, M. Riou, J. Torrejon, D. Ravelosona, W. Kang, W. Zhao, J. Grollier, D. Querlioz, Forecasting the outcome of spintronic experiments with neural ordinary differential equations. *Nat. Commun.* **13**, 1016 (2022).
14. K. Raab, M. A. Brems, G. Beneke, T. Dohi, J. Rothörl, J. H. Mentink, M. Kläui, Brownian reservoir computing realized using geometrically confined skyrmions. arXiv:2203.14720 [cond-mat.mtrl-sci] (28 March 2022).
15. K. M. Song, J.-S. Jeong, B. Pan, X. Zhang, J. Xia, S. Cha, T.-E. Park, K. Kim, S. Finizio, J. Raabe, J. Chang, Y. Zhou, W. Zhao, W. Kang, H. Ju, S. Woo, Skyrmion-based artificial synapses for neuromorphic computing. *Nat. Electron.* **3**, 148–155 (2020).
16. C. Chen, T. Lin, J. Niu, Y. Sun, L. Yang, W. Kang, N. Lei, Surface acoustic wave controlled skyrmion-based synapse devices. *Nanotechnology* **33**, 115205 (2022).
17. D. Pinna, F. A. Araujo, J.-V. Kim, V. Cros, D. Querlioz, P. Bessiere, J. Droulez, J. Grollier, Skyrmion gas manipulation for probabilistic computing. *Phys. Rev. Applied.* **9**, 064018 (2018).
18. J. Zázvorka, F. Jakobs, D. Heinze, N. Keil, S. Kromin, S. Jaiswal, K. Litzius, G. Jakob, P. Virnau, D. Pinna, K. Everschor-Sitte, L. Rózsa, A. Donges, U. Nowak, M. Kläui, Thermal skyrmion diffusion used in a reshuffler device. *Nat. Nanotechnol.* **14**, 658–661 (2019).
19. S. Fukami, C. Zhang, S. DuttaGupta, A. Kurenkov, H. Ohno, Magnetization switching by spin–orbit torque in an antiferromagnet–ferromagnet bilayer system. *Nat. Mater.* **15**, 535–541 (2016).
20. A. Kurenkov, S. Fukami, H. Ohno, Neuromorphic computing with antiferromagnetic spintronics. *J. Appl. Phys.* **128**, 010902 (2020).
21. M. Zahedinejad, H. Fulara, R. Khymyn, A. Houshang, M. Dvornik, S. Fukami, S. Kanai, H. Ohno, J. Åkerman, Memristive control of mutual spin Hall nano-oscillator synchronization for neuromorphic computing. *Nat. Mater.* **21**, 81–87 (2022).
22. A. Fert, V. Cros, J. Sampaio, Skyrmions on the track. *Nat. Nanotechnol.* **8**, 152–156 (2013).
23. N. Nagaosa, Y. Tokura, Topological properties and dynamics of magnetic skyrmions. *Nat. Nanotechnol.* **8**, 899–911 (2013).
24. S. Mühlbauer, B. Binz, F. Jonietz, C. Pfleiderer, A. Rosch, A. Neubauer, R. Georgii, P. Böni, Skyrmion lattice in a chiral magnet. *Science* **323**, 915–919 (2009).
25. X. Z. Yu, Y. Onose, N. Kanazawa, J. H. Park, J. H. Han, Y. Matsui, N. Nagaosa, Y. Tokura, Real-space observation of a two-dimensional skyrmion crystal. *Nature* **465**, 901–904 (2010).
26. N. Romming, C. Hanneken, M. Menzel, J. E. Bickel, B. Wolter, K. von Bergmann, A. Kubetzka, R. Wiesendanger, Writing and deleting single magnetic skyrmions. *Science* **341**, 636–639 (2013).
27. W. Jiang, P. Upadhyaya, W. Zhang, G. Yu, M. B. Jungfleisch, F. Y. Fradin, J. E. Pearson, Y. Tserkovnyak, K. L. Wang, O. Heinonen, S. G. E. te Velthuis, A. Hoffmann, Blowing magnetic skyrmion bubbles. *Science* **349**, 283–286 (2015).
28. G. Chen, A. Mascaraque, A. T. N'Diaye, A. K. Schmid, Room temperature skyrmion ground state stabilized through interlayer exchange coupling. *Appl. Phys. Lett.* **106**, 242404 (2015).
29. O. Boulle, J. Vogel, H. Yang, S. Pizzini, D. de Souza Chaves, A. Locatelli, T. O. Menteş, A. Sala, L. D. Buda-Prejbeanu, O. Klein, M. Belmeguenai, Y. Roussigné, A. Stashkevich, S. M. Chérif, L. Aballe, M. Foerster, M. Chshiev, S. Auffret, I. M. Miron, G. Gaudin, Room-temperature chiral magnetic skyrmions in ultrathin magnetic nanostructures. *Nat. Nanotechnol.* **11**, 449–454 (2015).
30. C. Moreau-Luchaire, C. Moutafis, N. Reyren, J. Sampaio, C. A. F. Vaz, N. Van Horne, K. Bouzehouane, K. Garcia, C. Deranlot, P. Warnicke, P. Wohlhüter, J.-M. George, M. Weigand, J. Raabe, V. Cros, A. Fert, Additive interfacial chiral interaction in multilayers for stabilization of small individual skyrmions at room temperature. *Nat. Nanotechnol.* **11**, 444–448 (2016).
31. S. Woo, K. Litzius, B. Krüger, M.-Y. Im, L. Caretta, K. Richter, M. Mann, A. Krone, R. M. Reeve, M. Weigand, P. Agrawal, I. Lemesh, M.-A. Mawass, P. Fischer, M. Kläui, G. S. D. Beach, Observation of room-temperature magnetic skyrmions and their current-driven dynamics in ultrathin metallic ferromagnets. *Nat. Mater.* **15**, 501–506 (2016).
32. Y. Paquo, F. Duport, A. Smerieri, J. Dambre, B. Schrauwen, M. Haelterman, S. Massar, Optoelectronic reservoir computing. *Sci. Rep.* **2**, 287 (2012).
33. D. Du, F. Cai, M. A. Zidan, W. Ma, S. H. Lee, W. D. Lu, Reservoir computing using dynamic memristors for temporal information processing. *Nat. Commun.* **8**, 2204 (2017).
34. Y. Zhong, J. Tang, X. Li, B. Gao, H. Qian, H. Wu, Dynamic memristor-based reservoir computing for high-efficiency temporal signal processing. *Nat. Commun.* **12**, 408 (2021).
35. Y. H. Jang, W. Kim, J. Kim, K. S. Woo, H. J. Lee, J. W. Jeon, S. K. Shim, J. Han, C. S. Hwang, Time-varying data processing with nonvolatile memristor-based temporal kernel. *Nat. Commun.* **12**, 5727 (2021).
36. R. Nakane, A. Hirose, G. Tanaka, Spin waves propagating through a stripe magnetic domain structure and their applications to reservoir computing. *Phys. Rev. Res.* **3**, 033243 (2021).
37. G. Milano, G. Pedretti, K. Montano, S. Ricci, S. Hashemkhani, L. Boarino, D. Ielmini, C. Ricciardi, In materia reservoir computing with a fully memristive architecture based on self-organizing nanowire networks. *Nat. Mater.* **21**, 195–202 (2022).
38. D. Marković, N. Leroux, M. Riou, F. A. Araujo, J. Torrejon, D. Querlioz, A. Fukushima, S. Yuasa, J. Trastoy, P. Bortolotti, J. Grollier, Reservoir computing with the frequency, phase, and amplitude of spin-torque nano-oscillators. *Appl. Phys. Lett.* **114**, 012409 (2019).
39. K. Takano, C. Sugano, M. Inubushi, K. Yoshimura, S. Sunada, K. Kanno, A. Uchida, Compact reservoir computing with a photonic integrated circuit. *Opt. Express* **26**, 29424–29439 (2018).
40. T. Hofmann, B. Schölkopf, A. J. Smola, Kernel methods in machine learning. *Ann. Stat.* **36**, 1171–1220 (2008).
41. S. Sugimoto, S. Kasai, E. Anokhin, Y. Takahashi, Y. Tokura, Nonequilibrium skyrmion accumulation induced by direct current in Ir/Co/Pt heterostructure. *App. Phys. Express* **12**, 073002 (2019).
42. T. Yokouchi, S. Sugimoto, B. Rana, S. Seki, N. Ogawa, S. Kasai, Y. Otani, Creation of magnetic skyrmions by surface acoustic waves. *Nat. Nanotechnol.* **15**, 361–366 (2020).
43. S. Sugimoto, W. Koshibae, S. Kasai, N. Ogawa, Y. Takahashi, N. Nagaosa, Y. Tokura, Nonlocal accumulation, chemical potential, and Hall effect of skyrmions in Pt/Co/Ir heterostructure. *Sci. Rep.* **10**, 1009 (2020).
44. Y. LeCun, L. Bottou, Y. Bengio, P. Haffner, Gradient-based learning applied to document recognition. *Proc. IEEE* **86**, 2278–2324 (1998).
45. W. Legrand, D. Maccariello, N. Reyren, K. Garcia, C. Moutafis, C. Moreau-Luchaire, S. Collin, K. Bouzehouane, V. Cros, A. Fert, Room-temperature current-induced generation and motion of sub-100 nm skyrmions. *Nano Lett.* **17**, 2703–2712 (2017).
46. F. Büttner, I. Lemesh, M. Schneider, B. Pfau, C. M. Günther, P. Hessing, J. Geilhufe, L. Caretta, D. Engel, B. Krüger, J. Viefhaus, S. Eisebitt, G. S. D. Beach, Field-free deterministic ultrafast creation of magnetic skyrmions by spin-orbit torques. *Nat. Nanotechnol.* **12**, 1040–1044 (2017).
47. S. Li, A. Du, Y. Wang, X. Wang, X. Zhang, H. Cheng, W. Cai, S. Lu, K. Cao, B. Pan, N. Lei, W. Kang, J. Liu, A. Fert, Z. Hou, W. Zhao, Experimental demonstration of skyrmionic magnetic tunnel junction at room temperature. *Sci. Bull.* **67**, 691–699 (2022).
48. A. K. Nayal, V. Kumar, T. Ma, P. Werner, E. Pippel, R. Sahoo, F. Damay, U. K. Rößler, C. Felser, S. S. P. Parkin, Magnetic antiskyrmions above room temperature in tetragonal Heusler materials. *Nature* **548**, 561–566 (2017).
49. S. Seki, M. Suzuki, M. Ishibashi, R. Takagi, N. D. Khanh, Y. Shiota, K. Shibata, W. Koshibae, Y. Tokura, T. Ono, Direct visualization of the three-dimensional shape of skyrmion strings in a noncentrosymmetric magnet. *Nat. Mater.* **21**, 181–187 (2022).

Acknowledgments

Funding: This work was supported by the JSPS Grants-in-Aid for Scientific Research (A) (grant nos. 18H03685, 20H00349, and 21H04440), Scientific Research (B) (grant no. 21H01794), and Young Scientists (grant no. 19 K14667); by JST PRESTO (grant nos. JPMJPR18L3, JPMJPR18L5, and JPMJPR17I3); by the Asahi Glass Foundation; and by the Murata Science Foundation. **Author contributions:** Y.O. and T.Y. conceived the project. S. Su and S.K. deposited the thin films. T.Y. fabricated the devices and conducted the measurements with assistance from B.R., Y.S., S. Se, and N.O. T.Y. analyzed the data and performed the calculation. T.Y. and Y.O. wrote the draft. All authors discussed the results and commented on the manuscript. **Competing interests:** The authors declare that they have no competing interests. **Data and materials availability:** All data needed to evaluate the conclusions in the paper are present in the paper and/or the Supplementary Materials.

Submitted 16 April 2022
Accepted 15 August 2022
Published 30 September 2022
10.1126/sciadv.abq5652

ScienceAdvances

Pattern recognition with neuromorphic computing using magnetic field–induced dynamics of skyrmions

Tomoyuki YokouchiSatoshi SugimotoBivas RanaShinichiro SekiNaoki OgawaYuki ShiomiShinya KasaiYoshichika Otani

Sci. Adv., 8 (39), eabq5652. • DOI: 10.1126/sciadv.abq5652

Science Advances (ISSN) is published by the American Association for the Advancement of Science. 1200 New York Avenue NW, Washington, DC 20005. The title *Science Advances* is a registered trademark of AAAS.